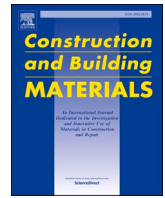




Contents lists available at ScienceDirect

Construction and Building Materials

journal homepage: www.elsevier.com/locate/conbuildmat

Analysis of load-bearing capacity factors of textile-reinforced mortar using multilayer perceptron and explainable artificial intelligence

Youngjae Song^a, Kwangsu Kim^a, Seunghee Park^{b,*}, Sun-Kyu Park^b, Jongho Park^{c,*}

^a College of Computing and Informatics, Sungkyunkwan University, Suwon 16419, Republic of Korea

^b Department of Civil, Architectural and Environmental System Engineering, Sungkyunkwan University, Suwon 16419, Republic of Korea

^c Global Frontiers of Resilient EcoSmart City, Sungkyunkwan University, Suwon 16419, Republic of Korea

ARTICLE INFO

Keywords:

TRM
Machine learning
Explainable artificial intelligence
Load-bearing capacity

ABSTRACT

With the aging of reinforced concrete structures, textiles, which are fiber composite materials, have been gaining attention for structural strengthening and replacement of steel reinforcements. The application of textile-reinforced mortar (TRM) is one method of strengthening structures using textiles. Various factors affect the performance when structures are strengthened with TRM; it is affected by the physical properties of the material, such as tensile strength and elongation, and external factors, which vary depending on the design condition, such as textile geometry and strengthening method. Therefore, it is necessary to develop an accurate method that considers the influence of various external factors for evaluating the load-bearing capacity in flexural of TRM-strengthened RC beam. A total of 100 experimental data were learned using a multilayer perceptron (MLP) deep learning model with 24 features, which were analyzed using explainable artificial intelligence, shapley additive explanations (SHAP). The MLP model exhibited a high performance, with a coefficient of determination of 0.9677, indicating the complex correlation between the given features. Regarding the influence of external factors on yield strength, the weft fiber spacing had a negative impact with high influence, and the warp fiber spacing was found to have a very low effect. The anchorage and the number of layers seemed to have a positive impact; however, the effect was small.

1. Introduction

The corrosion of steel reinforcements in concrete structures can shorten the life of the structures, deteriorate their performance, and cause accidents related to their collapse. Structural strengthening technology using fiber composite materials has been in practice for two decades because such materials are noncorrosive and have a high strength-to-weight ratio. In particular, because the development of manufacturing technology and increased production are expected to secure economic feasibility, the possibility of using various fiber composite materials has increased. Textile-reinforced mortar (TRM) is used for strengthening structures using textiles and inorganic matrices, such as mortar. Textiles are made from fibers, such as carbon, alkali-resistant (AR) glass, and aramid, woven into fabrics with perforations between the fibers. This is advantageous for ensuring the integrity of a structure

[1–3].

Many factors affect the performance of textiles in strengthened structures. A method for measuring the physical and mechanical properties (tensile strength, bond strength and so on) of TRM coupon specimens was presented in AC434 and adopted in ACI 549.4R [4,5]. In addition, various external factors other than physical and mechanical properties can affect the TRM performance such as textile geometry, anchorage, and number of layers.

In the case of textile geometry, D'Ambrisi and Focacci [6] find that strength increased with increasing thickness of fiber in transverse direction, but it could not conclude clear considering the in the range of experimental scatter [3]. Colombo et al. [7] found that delamination and crack propagation occurred in the weft direction when the weft spacing was small, the tension-stiffening effect increased as the weft spacing increased, and weft spacing variation not affects the load-

* Corresponding authors.

E-mail addresses: yuong13@skku.edu (Y. Song), kim.kwangsu@skku.edu (K. Kim), shparkpc@skku.edu (S. Park), skpark@skku.edu (S.-K. Park), rhapsode@skku.edu (J. Park).

¹ As a research director, he contributed to the selection of research topics and gave continuous advice in the process of writing the paper.

² He contributed to writing all the papers, including data collection, overview, and analysis of research results.

bearing capacity, but Park et al. [8] and Yin and Xu [9] found that the load-bearing capacity increased as the mesh size decreased because the weft fibers could serve as mechanical interlock for warp fibers. In the case of additional strengthening layer as anchor for TRM, Sneed et al., Escrig et al., and Raof et al. [10–12] reinforced structures using U-strips to improve the efficiency of the strengthening system; however, they found no evidence that the method could produce an increase in the load-carrying capacity. By contrary, Wakjira et al. [13] and Dai et al. [14] confirmed that the addition of side reinforcements imparted a better performance in improving the flexural strength and fracture modes, and Park et al. [8] used bolt anchors at both ends of a beam to prevent the slipping of textiles and to significantly improve the stiffness and yield flexural strength. Ombres, L. [15] confirmed that the flexural performance of FRCM-strengthened beams could be improved by securing an appropriate bond length. In the case of number of layers, it was found that flexural strength was increased when layer increased from 1 to 3 in Raof et al. [12], and 1 to 2 layers in Colombo et al. [7]. Tetta et al. [16] was also found that effectiveness of TRM jackets increased with increasing number of layers. However, Koutas et al. [3] summarized the effects of layer configuration in terms of the failure mode rather than the load-bearing capacity.

In addition, textile-based concrete composites exhibit complex behaviors, in which the strength and failure mode change according to the changes in various variables, such as textile geometry, curing method, size effect on tension hardening, bond strength, and prestress [7,17,18]. Many cases showed that different influences were exerted by the factors depending on the experimental environment. This phenomenon is because the experimental environment is limited, and many external factors as textile geometry and strengthening method affect the TRM. Therefore, it is necessary to establish an accurate performance evaluation system for designing the TRM strengthening method, and the evaluation process should consider various design factors of textiles. In these studies, the influence of external factors of the TRM on its performance was investigated through artificial intelligence (AI).

To overcome the problems of a limited experimental environment, prediction studies have been conducted on the performance of concrete composite members using AI. Nguyen et al. [19] proposed a model for predicting the effective moment of inertia using gene expression programming (GEP) to predict the deflection of reinforced concrete (RC) beams reinforced with FRP. Taha et al. [20] performed a parametric study using backpropagation neural networks (BPNNs) to reflect the nonlinearity of FRPs, which affects the strength of the members. Naderpour et al. [21] used the group method of data handling to predict the moment capacity of ferrocement composites, and the predicted results were compared with those obtained using BPNNs, an adaptive neuro-fuzzy inference system, GEP, and traditional equations. To solve the problems regarding limited data and limited mechanical and physical insights into the prediction of the structural behavior and lifetime of textile-reinforced concrete (TRC), recurrent neural networks based on neural networks and time-dependent measurements or numerical analysis have been introduced [22–24]. Neural networks have also been introduced to predict the flexural strength of TRC [25,26] and to determine the parameters of the bond model for FRCMs [27]. Wakjira et al. [28] compared seven machine learning and four existing analytical models for verifying a data-driven approach to determine the load and flexural capacities of FRCMs with feature on physical properties. The extreme gradient boosting (XGBoost) model showed better prediction ability compared with other machine learning and existing models, and the resistance reduction factor based on the XGBoost model was proposed to assess the functionality and performance of the structure with FRCMs.

There are still insufficient cases of using AI to evaluate the behavior of structures, and the scope of the research is limited. Therefore, in this study, based on the experimental data of a TRM-strengthened RC beam, the load-bearing capacity in flexural was evaluated through AI, and various strength-influencing factors, called load-bearing capacity factors

in this study, were analyzed using explainable AI (XAI). Thus, the potential of AI as a tool for the performance prediction and designing of structures was reviewed.

2. Deep neural networks

2.1. Artificial neural network

An artificial neural network (ANN) is an AI tool that is inspired by the behavior of the human brain. It is known that a neural network can “learn” the representation of given data or solutions to a given task. To learn such information, a neural network determines the weights embedded in it such that the weights sufficiently represent the given data or solve the given task. The learning procedure using a deep neural network is called “deep learning”. Most modern deep learning algorithms are based on an optimization algorithm called the gradient descent to determine such weights. More specifically, deep learning algorithms consist of a model, an optimization algorithm, an error (loss) function, and a dataset; a model (i.e., a neural network) is optimized (learned) by an optimization algorithm to reduce the error (from an error function) between the target and output values obtained from the given input data (a dataset).

It has been proven mathematically that a deep neural network with more than one hidden layer can learn (approximate) any complex function using the universal approximation theorem [29]. Therefore, a deep neural network is an appropriate model to predict load-bearing capacity while considering the complex relationship between features.

2.2. XAI

Deep neural networks are widely accepted in high-stake AI systems, such as autonomous driving, healthcare, and military systems [30]. Compared with traditional rule-based systems, these AI models perform remarkably well in predicting. However, identifying why deep neural networks provide such a prediction is still challenging because of their black-box nature; we do not know which part of the input data contributes to a certain prediction. Thus, explaining a given prediction by a deep neural network is indispensable to understanding its behavior and extracting interpretable knowledge.

The contribution of each feature to the given prediction of load-bearing capacity is not specified in a deep neural network. Furthermore, additional components such as TRM should be clearly specified to determine which properties affect the flexural performance and guarantee safety. Hence, the XAI method is a state-of-the-art technique (when using a deep neural network as a predictor) to analyze the relationship between the TRM properties and predicted load-bearing capacity.

3. Experimental program

3.1. Data

The input features are presented in Table 1. Twenty-four features were determined by classifying the common or comparable features referred from 13 studies that evaluated under similar experimental conditions. Out of the 24 features, 12 features were related to RC and 11 features were related to textiles. The feature of textile is divided two parts, one is material type of textile and the other one is design factors of TRM. Yield strength of the TRM-strengthened RC beam was included as a performance index and inference target. A total of 100 input data points were derived, as shown in Appendix A. There was not included the bond strength in dataset because the properties of mortar were omitted in some studies. Therefore, AI learning was conducted assuming that there was no problem with bond between RC subtract and TRM.

Table 1
Input features.

Feature		Description
Design factors of RC	$b(mm)$	Beam width
	$h(mm)$	Beam height
	$d_t(mm)$	Effective depth of tension rebar
	$d_c(mm)$	Effective depth of compression rebar
	$A_s(mm^2)$	Area of tension rebar
	$A'_s(mm^2)$	Area of compression rebar
	$f_{ck}(MPa)$	Compressive strength at 28 days of concrete
	$f_y(MPa)$	Yield strength of tension rebar
	$f'_y(MPa)$	Yield strength of compression rebar
	$L(mm)$	Length of RC beam
	$l(mm)$	Clear span of RC beam
	$a(mm)$	Distance between support and loading point
	Material type of textile	C
B		Basalt
G		Glass and alkali-resistant (AR) glass
PBO		Poliparafenilenbenzobisoxazole
CF		Carbon fiber-reinforced polymer
Design factors of TRM	$A_f(mm^2)$	Total cross-section area of textile in TRM
	$f_f(MPa)$	Tensile strength of fiber in textile
	$S_{wf}(mm)$	Spacing of weft fiber
	$S_{wr}(mm)$	Spacing of warp fiber
	Layer	Number of layers
Strength	Anchorage	Status of additional strengthening
	$P_y(kN)$	Yield strength that loads at rebar yield on flexural behavior

3.1.1. Preprocessing

Before training our deep neural network model, the feature values were aligned within an identical distribution for better convergence [31]. We tested three different types of scalers: standard, robust, and min-max scalers. A standard scaler scales feature values into a standardized normal distribution. A robust scaler, proposed in statistics, is robust against outliers. The min-max scaler transforms the minimum feature value into zero and the maximum feature value into one. After implementing these three scalers in an independent manner, the performance was found to be the highest when using the standard scaler. Hence, all the experiments described below were conducted using a standard scaler.

For the train/test split, we implemented stratified sampling to prevent a biased split [32]. The distribution of the train/test set in the feature space should overlap so that representatives learned from the training dataset are applicable to the test set, which leads to credible evaluation results that are well aligned to the distribution of the training dataset. Finally, train data and test data were split in an 8:2 ratio for our experimental setup.

3.2. Evaluation model

3.2.1. Multi-layer perceptron (MLP)

An MLP is composed of an input layer, hidden layers, and an output layer as shown in Fig. 1. Each layer is operated by a pile of perceptrons (in width) that compute the weighted sum of the given inputs and then convey the output signals through a predefined nonlinear activation function. The deeper and wider a neural network, the more complex the network; hence, the model eventually has the capability to learn more complex representations from the input data. The details of our model are as follows.

The weights were initialized using the Xavier uniform initializer [33] before the model was trained. As the Xavier uniform initializer with the ReLU(Rectified Linear Unit) activation function [34] frequently fails to converge in deep neural networks [35], the ELU(Exponential Linear Unit) activation function proposed by Clevert et al. [36] was used between every layer in the MLP model. The dimensions of each layer are listed in Table 2.

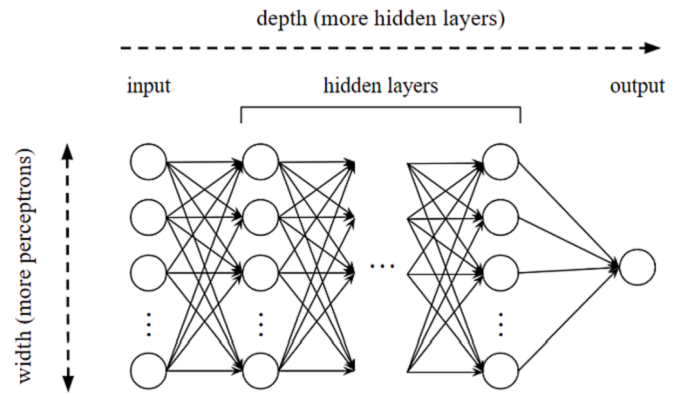


Fig. 1. Schematic of an MLP.

3.2.2. Backpropagation by gradient descent

Given a neural network model and a predefined loss function, the weights of the model are optimized to predict the target output by reducing the loss between the predicted value and target output. The method of optimizing the weights using the gradient of the loss function with respect to the weights is known as gradient descent. As the gradient calculated using the gradient descent method is propagated backward from the output layer to the input layer, all weights along the path through which the loss gradient passes are updated so that the predicted value approaches the target output.

The Adam optimizer [37] was used to train the MLP model. Adam is a state-of-the-art optimizer that guarantees fast and robust learning and a high accuracy in almost all cases. We used the mean squared error (MSE) as the loss function. It is expressed as follows:

$$MSE = \frac{1}{N} \sum_{i=1}^N (y_i - \hat{y}_i)^2, \tag{1}$$

where N denotes the number of data points, y_i denotes the target output, and \hat{y}_i denotes the predicted output value. Our MLP model attempts to optimize weights using the backpropagation algorithm with the Adam optimizer, such that the error between the predicted and target outputs is as low as possible.

3.3. XAI model

Recently, various methods have been proposed to help researchers and end users understand the predictions from deep neural networks. Among them, Shapley Additive exPlanations (SHAP) [38] is regarded as one of the most trustworthy frameworks that exploits the Shapley value concept from game theory [39]. A Shapley value is assigned to each feature for calculating the contribution value of the feature to a given prediction. In the Shapley value method, each feature value of a data sample and the corresponding prediction are assumed to be a player and the result of a game, respectively. As game theory seeks the contribution of each player to the result, the Shapley value method can be used to identify the contribution of each feature value to the prediction.

SHAP was used to explain our AI model by unifying the Shapley value with previously proposed explanation methods (LIME [40] and

Table 2
Dimensions of the MLP model.

Layer type	Dimension
Input layer	23 (Number of input features)
Hidden layer 1	1024
Hidden layer 2	512
Hidden layer 3	512
Hidden layer 4	256
Output layer	1 (Predicted yield strength)

DeepLIFT [41]), owing to the implausible amount of computation required. Eventually, one can determine which TRM properties are crucial, and which are not for load-bearing capacity prediction.

3.3.1. Additive feature attribution methods

$$g(z') = \phi_0 + \sum_{i=1}^M \phi_i z'_i \quad (2)$$

Here, $z' \in \{0, 1\}^M$, M is the number of input features, $g(z')$ represents the explanation function for a given feature z' , and $\phi_i \in \mathbb{R}$; ϕ_0 denotes the ground value when any input feature does not participate in the prediction, and ϕ_i represents the contribution of the i^{th} input feature, z'_i , to the prediction. Equation (2) shows the associated contribution of each input feature while considering its presence or absence.

3.3.2. DeepLIFT

DeepLIFT has been proposed as an additive explanation method. DeepLIFT is established based on the property called “summation-to-delta”, as below:

$$\sum_{i=1}^n C_{\Delta x_i \Delta o} = \Delta o, \quad (3)$$

Here, $C_{\Delta x_i \Delta o}$ represents the contribution of the specific input feature Δx_i with respect to the total variation in the prediction Δo . Equation (3) indicates that the sum of each contribution when a specific input feature is perturbed should be the same as the total variation in the prediction. In other words, the change in the prediction score is only affected by the change in the input features.

3.3.3. DeepSHAP

DeepLIFT associated with the Shapley value is called DeepSHAP. We used DeepSHAP to quantify the effect of each property of TRM on the yield strength. f denotes the original predictor to be explained, and $f(x)$ denotes the prediction score of a predictor for a single input sample x .

$$\phi_i = \sum_{S \subseteq F \setminus \{i\}} \frac{|S|!(|F| - |S| - 1)!}{|F|!} [f_{S \cup \{i\}}(x_{S \cup \{i\}}) - f_S(x_S)] \quad (4)$$

In Equation (4), the contribution value is calculated using the Shapley value. The Shapley value considers all possible combinations of features and the corresponding prediction values ($f(x)$) for the given combination of features. S denotes the feature subset, F denotes the full feature set, and x_S denotes the input data when only the features in S participate during the inference process. Intuitively, if the prediction score is consistently high when a certain input feature is present during inference, the feature should also have a high contribution value. In further experiments, we used DeepSHAP as an explainer.

4. Results and discussion

4.1. Prediction performance

MLP model was compared with machine learning techniques [42], such as the support vector machine (SVM), K-nearest neighbors (KNN), decision tree, and random forest, as shown in Table 3, to demonstrate its suitability for predicting the complex behavior of TRM. Mean Absolute Error (MAE) and Root Mean Square Error (RMSE) for the metrics were

Table 3
Evaluation results.

Model	MAE	RMSE	R^2
SVM	5.3526	7.9312	0.9004
KNN	595.954	165.8566	0.5012
Decision Tree	4.67	7.1483	0.9443
Random Forest	4.737	6.368	0.9454
MLP	3.6924	5.0211	0.9677

selected as well as R^2 . The lower MAE and RMSE are, the better models perform.

$$MAE = \frac{1}{N} \sum_{i=1}^N |y_i - \hat{y}_i|, \quad (5)$$

$$RMSE = \sqrt{\frac{1}{N} \sum_{i=1}^N (y_i - \hat{y}_i)^2}, \quad (6)$$

where N denotes the number of data points, y_i denotes the target output, and \hat{y}_i denotes the predicted output value.

R^2 score is popular metric for evaluating the performance of regression models. R^2 score can span from 0 to 1. The closer to 1, the better the regression models fit.

$$R^2 = 1 - \frac{\sum_{i=1}^N (y_i - \hat{y}_i)^2}{\sum_{i=1}^N (y_i - \bar{y})^2}, \quad (7)$$

where \bar{y} denotes the average of target values in the dataset.

KNN presented an unusable level of prediction. Meanwhile, the SVM method exhibited a decent performance; however, the decision tree and random forest models showed slightly better performances in evaluating the load-bearing capacity with mechanical-based data. The MLP model exhibited the best performance for a given regression problem; therefore, it was suitable for predicting the load-bearing capacity of TRM and was the best model for reflecting the complex correlation between the given features. Therefore, all subsequent impact analyses were conducted using the results of the MLP model.

Fig. 2 depicts the prediction curve by trained MLP model and target plots in both training and testing sets. The horizontal axis and vertical axis stand for an index of a sample and target feature respectively. If the blue curve is well-overlapped to the red curve, it means that trained MLP model performs well. In a usual supervised training setup like in this experiment, the model was expected to capture generalized patterns (not biased one to training sets) although it is trained only by partial dataset, namely training sets. If the trained model could have learnt patterns of unseen testing sets, it would indicate that the trained model was regarded as a generalized model representing the pattern of the given dataset. The prediction curves were fitted to target curves in both training and testing sets consistently, that is, it was shown that trained model have learnt generalized behavior of TRM structure. Hence, in order to reveal the complex behavior of a TRM structure, Fig. 2 justifies that it is reasonable to analyze learnt behavior by trained model instead of analyzing a genuine TRM structural behavior directly.

4.2. Feature influence

The average value and impact of each SHAP test sample are shown in Figs. 3 and 4, respectively. From Fig. 3, one can observe that the features related to the existing RC members have a significant influence on the load-bearing capacity. The TRM-related features affecting the load-bearing capacity, in decreasing order of significance, were the fiber tensile strength, cross-sectional area, weft fiber spacing, anchorage, number of layers, and warp fiber spacing. From Fig. 4, it presents three-dimensional graph plotting feature impacts in the form of SHAP values for each testing data (a dot). The horizontal axis and vertical axis stand for a list of features (sorted by an average impact magnitude) and SHAP value, respectively. The feature value is presented in the form of colors. The feature has global positive relation to the yield strength if the color changes from blue to red rightward, and global negative relation for leftward changes. If the feature does not have explicit relation to the yield strength, the color will change arbitrary. In addition, the variance (a width of dots distribution) approximately tells us how big the impact magnitude is. Larger SHAP values means the feature value contributes to the yield strength more, vice versa. Accordingly, impact of the feature

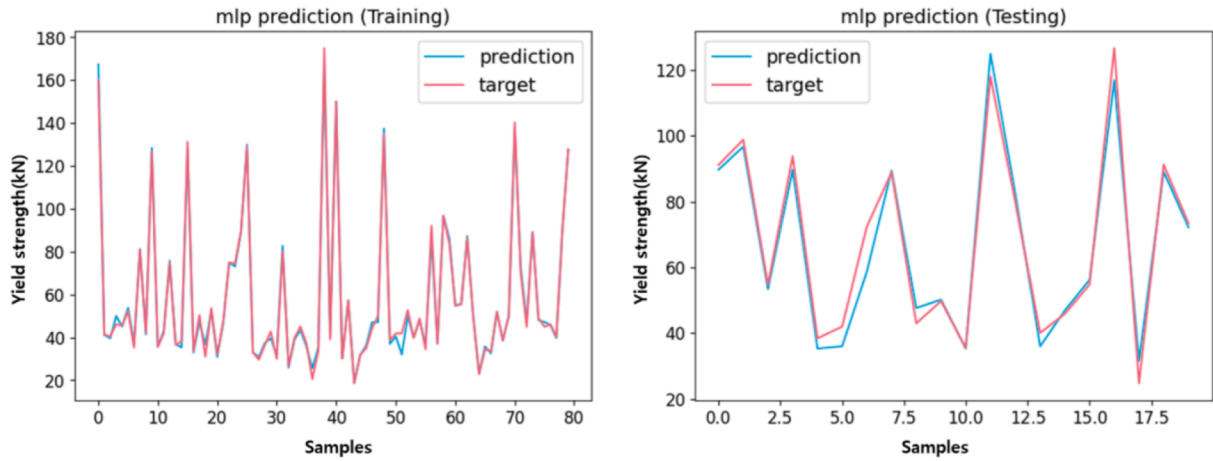


Fig. 2. Prediction and target values in both training and test sets.

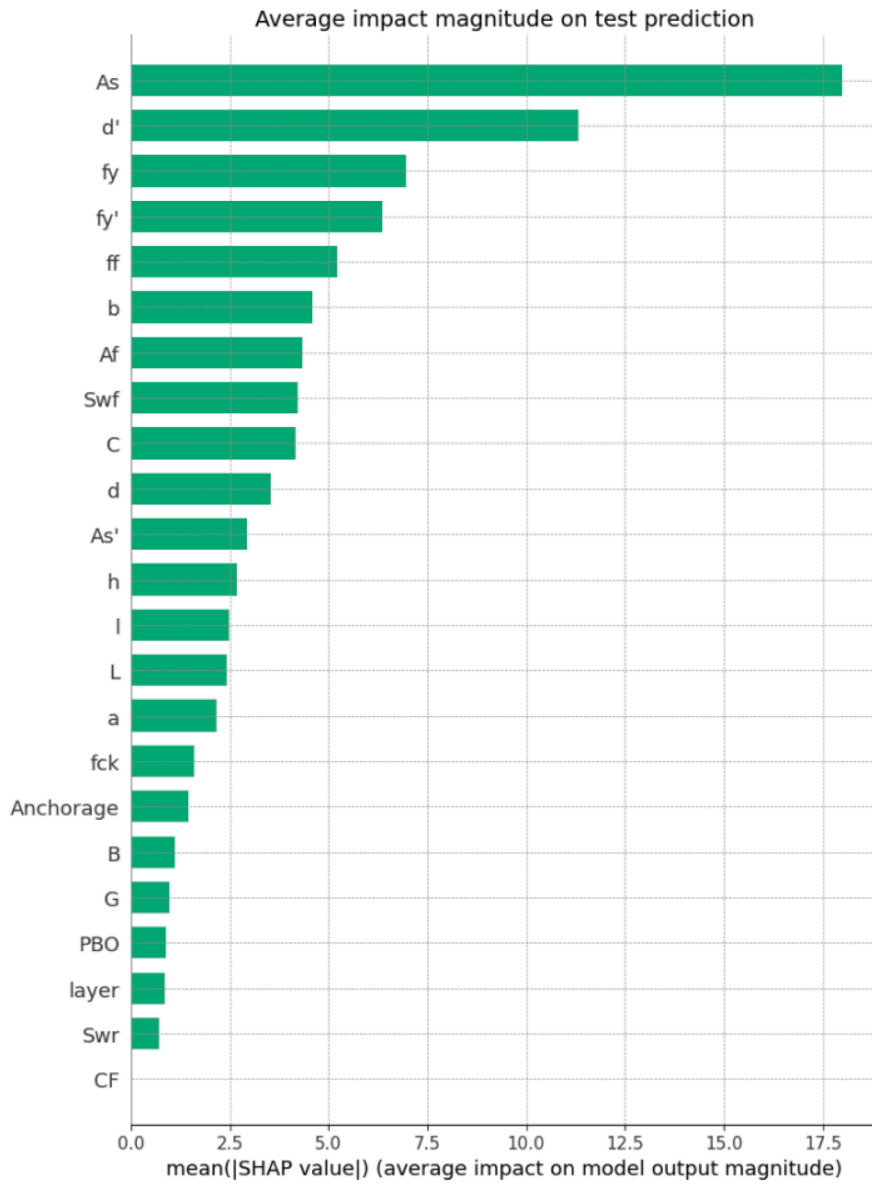


Fig. 3. Average impact magnitude on test set.

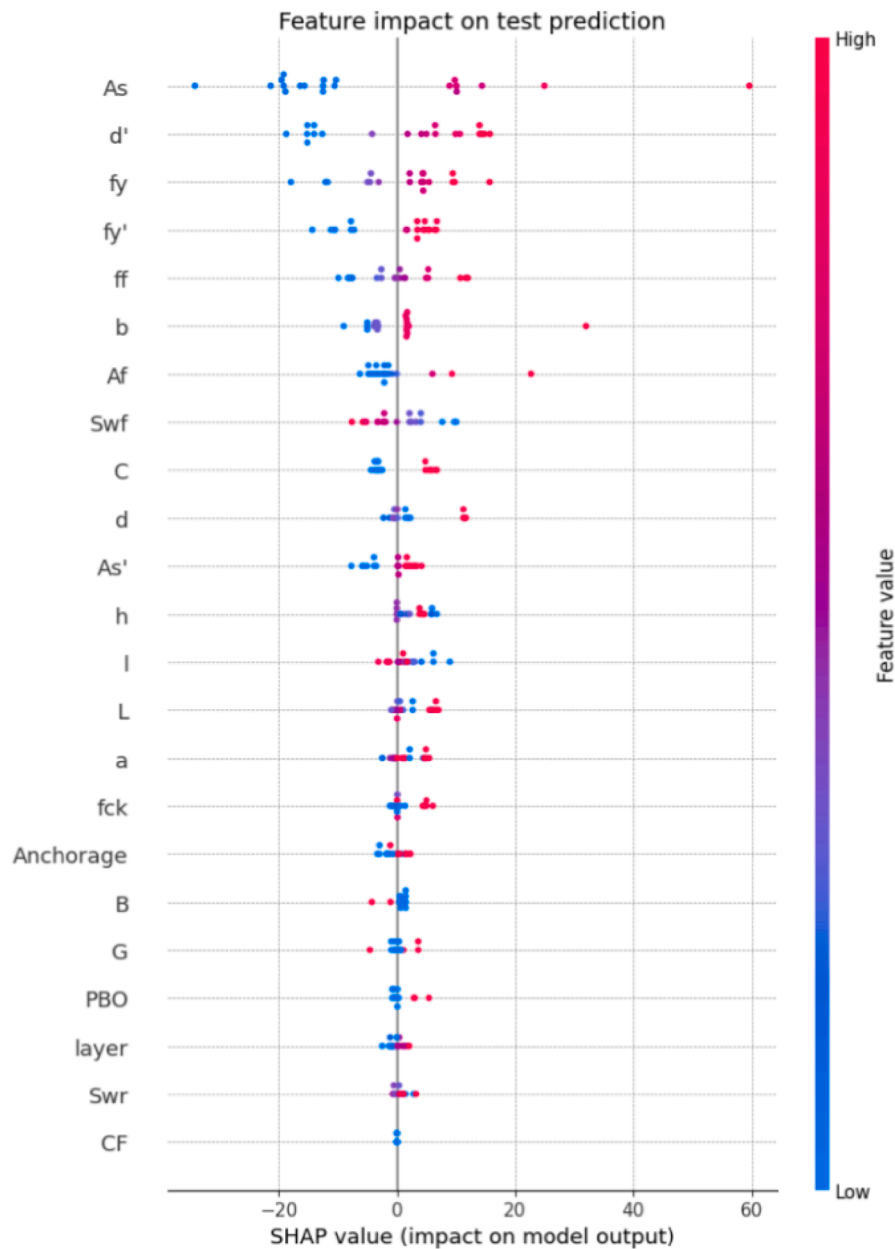


Fig. 4. Feature impact on each test sample.

can be determined and which relation the feature has, positive or negative. Therefore, one can observe that the features having a positive impact are the fiber tensile strength and cross-sectional area, and the feature having a negative impact is the weft fiber spacing. Anchorage and the number of layers seem to have a positive impact; however, the effect is small. Warp fiber spacing exerts a considerably low influence, and its impact is neither positive nor negative.

The effect of the type of textile material was the greatest when carbon was used, but it is difficult to determine the feature impact accurately because the rest of the materials do not have sufficient data. As an alternative, the type of materials is closely related to the tensile strength of the fiber, and the impact of tensile strength instead of materials can be considered until sufficient datasets for materials are accumulated.

4.3. Discussion

The ordinary physical properties of the material and the structural

geometry were used to calculate the strength of the RC structures. In addition, externally bonded reinforcements, such as FRP or TRM, for strengthening structures may require a model to analyze the bond strength between the concrete and strengthening materials. External factors, excluding material properties, particularly textile geometry, are also highly likely to affect textile performance. These factors are summarized in ACI 549.4R with the properties of the material [5] and a state-of-the-art review by Koutas et al. [3], which provides guidelines for the design of TRM as follows.

The ACI 549.4R [5] was the first established design guideline for FRCM strengthening. The design parameters of the constituent materials in FRCM are drying shrinkage, void content, tensile properties, bond and interlaminar shear strengths, matrix properties, and durability (aging, freezing and thawing, and fuel resistance) based on AC434 [4]. In addition, it was suggested that the open area of the textile mesh should occupy at least 33.3 % of the total area.

According to Koutas et al. (2019) [3], the factors causing a change in

Table 4
Comparison of the external factors for flexural strength of TRM.

External design factors of TRM	ACI 549.4R [5]	State-of-the-art (2019) [3]	This study
Geometry	At least 33.3 % of open area	No clear results	- Weft spacing has negative impact with high influence - Warp spacing has a low influence Low positive impact
Anchorage	Can be effective, but should be substantiated by the licensed design professional	No strong evidence	
Number of layers	Multilayer FRCM may necessary the longer values of development length.	More than one layer can alter the failure mode with slippage of the fiber.	

performance are the internal steel reinforcement ratio, polymer adhesive coating on textiles, and mortar type. It was found that the flexural performance either improved or deteriorated with respect to the amount of textile reinforcement. This is because the textile reinforcement leads to a change in the failure mode according to the changes in the textile layer. With respect to textile geometry and anchorage factors, no strong evidence that indicated a change in performance was found. In particular, it did not conform to the hypothesis that textiles would have a mechanical interlocking effect owing to mesh perforation.

A comparison of the external factors of TRM, based on the current guidelines and the results of this study, is shown in Table 4. The ACI 549.4 R [5] guidelines can be used to understand the minimum effect of each factor, and if necessary, an additional examination is required. State-of-the-art reviews [3] have not provided clear evidence of each effect. In this study, although the specific criteria suggested in ACI 549.4R [5] could not be analyzed, the specific effects of textile geometry, anchorage, and number of layers could be identified.

5. Conclusion

In this study, the flexural load-bearing capacity was evaluated through AI based on the experimental data of an RC beam strengthened with a TRM, and the load-bearing capacity factors were analyzed.

(1) The MLP model had a better regression performance than traditional machine learning, even though the training dataset was small, and effectively reflected the complex correlation between the given features.

(2) The external factors affecting the load-bearing capacity as textile geometry, anchorage, and the number of layers were analyzed. The spacing of the weft fibers had a negative impact, whereas the spacing of the warp fibers had a lower impact than other design factor of TRM. The anchorage and number of textile reinforcement layers had a positive impact; however, the effect was small.

(3) The results of learning and analyzing the load-bearing capacity of the TRM using the MLP model presented evidence to support the existing research results on textiles. However, feature impacts computed by SHAP values can only be a tool to compare the contributions of features

relatively and to identify the tendency of features whether they are in positive or negative relation to the target feature. Due to the lack of even more sophisticated analysis technique, absolute quantitative measurement remains as a challenging task.

This study was conducted by collecting data from a study based on the TRM in a similar experimental environment. By introducing AI technology for the evaluation of the strength of structures, it is possible to present evidence to analyze the load-bearing capacity factors whose influence is unclear. Therefore, it is necessary to develop a universal structural performance evaluation model through the expansion of experimental data that can be used to analyze different types of textile properties in future.

CRedit authorship contribution statement

Youngjae Song: Methodology, Software, Validation, Investigation, Writing – original draft, Writing – review & editing. **Kwangsu Kim:** Funding acquisition. **Seunghee Park:** Project administration, Supervision. **Sun-Kyu Park:** Supervision, Resources. **Jongho Park:** Conceptualization, Methodology, Validation, Formal analysis, Investigation, Data curation, Writing – original draft, Writing – review & editing.

Declaration of Competing Interest

The authors declare that they have no known competing financial interests or personal relationships that could have appeared to influence the work reported in this paper.

Data availability

Data are provided in Appendix A in manuscript.

Acknowledgment

This study was supported by the AI Convergence Research Fund, Sungkyunkwan University, 2021.

Appendix A Input data

Refs	b (mm)	h (mm)	d (mm)	d' (mm)	L (mm)	l (mm)	a (mm)	f _{ck} (MPa)	A _s (mm ²)	f _y (MPa)	A _s ' (mm ²)	f _y ' (MPa)	Material	f _f (MPa)	A _f (mm ²)	layer	S _{wr} (mm)	S _{wf} (mm)	Anchorage	P _y (kN)
[6]	400	250	200	50	2400	2200	750	40	461.8	523.15	461.8	523.15	RC							134.8
	400	250	200	50	2400	2200	750	40	461.8	523.15	461.8	523.15	RC							140.3
	400	250	200	50	2400	2200	750	40	461.8	523.15	461.8	523.15	Carbon	3051	31.96	2	10	10	0	160
	400	250	200	50	2400	2200	750	40	461.8	523.15	461.8	523.15	Carbon	3051	31.96	2	10	10	0	175
[43]	150	250	209	41	2400	2200	850	30	157.1	500	100.5	500	RC							39.8
	150	250	209	41	2400	2200	850	30	157.1	500	100.5	500	Carbon	4800	5	2	10	10	1	49
	150	250	209	41	2400	2200	850	30	157.1	500	100.5	500	Carbon	4800	7.5	3	10	10	1	51.8
	150	250	209	41	2400	2200	850	30	157.1	500	100.5	500	Carbon	4800	5	2	10	10	1	48.8
	150	250	209	41	2400	2200	850	30	157.1	500	100.5	500	PBO	5800	6.3	2	15	20	1	44.2
	150	250	209	41	2400	2200	850	30	157.1	500	100.5	500	Glass	2600	10.6	4	14.2	18.2	1	46.1
	150	250	209	41	2400	2200	850	30	314.2	500	100.5	500	RC							73.4
	150	250	209	41	2400	2200	850	30	314.2	500	100.5	500	Carbon	4800	5	2	10	10	1	86.2

(continued on next page)

(continued)

Refs	b (mm)	h (mm)	d (mm)	d' (mm)	L (mm)	l (mm)	a (mm)	f_{ck} (MPa)	A_s (mm ²)	f_y (MPa)	A_s' (mm ²)	f_y' (MPa)	Material	f_f (MPa)	A_f (mm ²)	layer	S_{wr} (mm)	S_{wf} (mm)	Anchorage	P_y (kN)
	150	250	209	41	2400	2200	850	30	314.2	500	100.5	500	Carbon	4800	7.5	3	10	10	1	89.2
	150	250	209	41	2400	2200	850	30	314.2	500	100.5	500	PBO	5800	6.3	2	15	20	1	92.1
	150	250	209	41	2400	2200	850	30	314.2	500	100.5	500	PBO	5800	6.3	2	15	20	1	83.7
	150	250	209	41	2400	2200	850	30	314.2	500	100.5	500	Glass	2600	5.3	2	14.2	18.2	1	74.6
	150	250	209	41	2400	2200	850	30	314.2	500	100.5	500	Glass	2600	5.3	2	14.2	18.2	1	70.5
	150	250	209	41	2400	2200	850	50	157.1	500	100.5	500	RC							42
	150	250	209	41	2400	2200	850	50	157.1	500	100.5	500	Carbon	4800	7.5	3	10	10	1	50.2
	150	250	209	41	2400	2200	850	50	157.1	500	100.5	500	PBO	5800	5	2	15	20	1	45.5
[44]	170	300	260	40	3000	2700	900	28	157.1	480	157.1	480	RC							22.8
	170	300	260	40	3000	2700	900	28	157.1	480	157.1	480	CFRP	4300	1.8	1	17	33	0	20.5
	170	300	260	40	3000	2700	900	28	157.1	480	157.1	480	CFRP	4300	3.6	2	17	33	0	41.9
	170	300	260	40	3000	2700	900	28	157.1	480	157.1	480	CFRP	4300	5.4	3	17	33	0	31
	170	300	260	40	3000	2700	900	28	157.1	480	157.1	480	CFRP	4300	2.7	1	17	33	0	26.7
	170	300	260	40	3000	2700	900	28	157.1	480	157.1	480	CFRP	4300	5.4	2	17	33	0	33.6
	170	300	260	40	3000	2700	900	28	157.1	480	157.1	480	CFRP	4300	8.1	3	17	33	0	36.4
[13]	500	300	263	20	2100	1900	950	30	157.1	515	100.5	535	Carbon	4800	14.1	2	10	10	1	81
	500	300	263	20	2100	1900	950	30	157.1	515	100.5	535	Glass	2600	14.1	2	14	18	0	55.3
	500	300	263	20	2100	1900	950	30	157.1	515	100.5	535	Glass	2600	14.1	2	14	18	1	55.1
	500	300	266	20	2100	1900	950	30	402.1	595	100.5	535	Carbon	4800	14.1	2	10	10	1	150
	500	300	266	20	2100	1900	950	30	402.1	595	100.5	535	Glass	2600	14.1	2	14	18	1	126.7
[45]	200	300	252.5	0	4000	3800	1275	21.4	353.4	440	0	0	RC							54.8
	200	300	252.5	0	4000	3800	1275	21.4	353.4	440	0	0	Carbon	3000	9.2	1	20	20	1	54.8
	200	300	252.5	0	4000	3800	1275	21.4	353.4	440	0	0	Carbon	2800	32.4	1	15	30	0	53.6
	200	300	252.5	0	4000	3800	1275	21.4	353.4	440	0	0	Carbon	2800	32.4	1	15	30	1	52.2
	200	300	252.5	0	4000	3800	1275	21.4	353.4	440	0	0	Carbon	2800	97.2	3	15	30	1	72.4
	200	300	247.5	0	4000	3800	1275	21.4	981.7	458	0	0	RC							127.8
	200	300	247.5	0	4000	3800	1275	21.4	981.7	458	0	0	Carbon	3000	9.2	1	20	20	1	126.8
	200	300	247.5	0	4000	3800	1275	21.4	981.7	458	0	0	Carbon	2800	32.4	1	15	30	0	118
	200	300	247.5	0	4000	3800	1275	21.4	981.7	458	0	0	Carbon	2800	32.4	1	15	30	1	131.2
	200	300	247.5	0	4000	3800	1275	21.4	981.7	458	0	0	Carbon	2800	97.2	3	15	30	1	129
[14]	120	150	130	0	960	860	355	30	157.1	210	0	0	RC							18.6
	120	150	130	0	960	860	355	30	157.1	210	0	0	Carbon	4362	4.84	1	10	10	0	30
	120	150	130	0	960	860	355	30	157.1	210	0	0	Carbon	4362	4.84	1	10	10	0	24.8
	120	150	130	0	960	860	355	30	157.1	210	0	0	Carbon	4362	9.68	2	10	10	0	33
	120	150	130	0	960	860	355	30	157.1	210	0	0	Carbon	4362	10.56	2	10	10	1	42
	120	150	130	0	960	860	355	30	157.1	210	0	0	Carbon	4362	4.84	1	10	10	0	31.9
	120	150	130	0	960	860	355	30	157.1	210	0	0	Carbon	4362	9.68	2	10	10	0	33.7
[46]	150	200	164	36	2200	2000	800	20	157.1	372	157.1	372	RC							37.18
	150	200	164	36	2200	2000	800	20	157.1	372	157.1	372	RC							34.39
	150	200	164	36	2200	2000	800	20	157.1	372	157.1	372	Basalt	623	256	10	25	25	1	45.89
	150	200	164	36	2200	2000	800	20	157.1	372	157.1	372	Basalt	623	128	5	25	25	1	40.12
	150	200	164	36	2200	2000	800	20	157.1	372	157.1	372	Basalt	623	256	10	25	25	1	46.98
[47]	150	250	216	33	3000	2700	900	22.77	339.3	515.44	157	521.89	RC							74.85
	150	250	216	33	3000	2700	900	22.77	339.3	515.44	157	521.89	PBO	5800	6.75	1	10	20	0	80.1
	150	250	216	33	3000	2700	900	22.77	339.3	515.44	157	521.89	PBO	5800	6.75	1	10	20	0	80.04
	150	250	217	32	3000	2700	900	23.02	157	525.9	100.53	535.6	RC							41.83
	150	250	217	32	3000	2700	900	23.02	157	525.9	100.53	535.6	PBO	5800	6.75	1	10	20	0	45.03
	150	250	217	32	3000	2700	900	23.02	157	525.9	100.53	535.6	PBO	5800	13.5	2	10	20	0	50.4
	150	250	217	32	3000	2700	900	23.02	157	525.9	100.53	535.6	PBO	5800	13.5	2	10	20	0	50.01
	150	250	217	32	3000	2700	900	23.02	157	525.9	100.53	535.6	PBO	5800	20.25	3	10	20	0	52.74
	150	250	217	32	3000	2700	900	23.02	157	525.9	100.53	535.6	PBO	5800	20.25	3	10	20	0	46.1
	150	250	217	32	3000	2700	900	22.39	157	525.9	100.53	535.6	PBO	5800	13.5	2	10	20	0	39.84
	150	250	217	32	3000	2700	900	22.39	157	525.9	100.53	535.6	PBO	5800	13.5	2	10	20	0	44.94
	150	250	217	32	3000	2700	900	22.39	157	525.9	100.53	535.6	PBO	5800	20.25	3	10	20	0	49.77
[12]	101	202	175	29	1675	1500	580	19.9	100.5	569	226.2	561	RC							30.1
	101	202	175	29	1675	1500	580	19.9	100.5	569	226.2	561	Carbon	1518	9.69	1	10	10	0	35.6
	101	202	175	29	1675	1500	580	19.9	100.5	569	226.2	561	Carbon	2843	9.69	1	10	10	0	37
	101	202	175	29	1675	1500	580	19.9	100.5	569	226.2	561	Carbon	1518	29.07	3	10	10	0	43
	101	202	175	29	1675	1500	580	19.9	100.5	569	226.2	561	Carbon	1518	48.45	5	10	10	0	57.2
	101	202	175	29	1675	1500	580	19.9	100.5	569	226.2	561	Basalt	1190	26.5	7	25	25	0	38.5
	101	202	175	29	1675	1500	580	19.9	100.5	569	226.2	561	Glass	794	31.42	7	12	12	0	40.2
	101	202	175	29	1675	1500	580	21.7	100.5	569	226.2	561	Carbon	1518	29.07	3	10	10	1	41.3
[15]	150	250	217	33	3000	2700	900	27.73	157	535.6	100.53	535.6	RC							39.1
	150	250	217	33	3000	2700	900	27.73	157	535.6	100.53	535.6	PBO	5800	13.5	2	10	20	0	44.94
	150	250	217	33	3000	2700	900	27.73	157	535.6	100.53	535.6	PBO	5800	20.25	3	10	20	0	49.77
[11]	200	500	450	50	4400	4000	1300	48.1	157	517.2	157	517.2	RC							74.86
	200	500	450	50	4400	4000	1300	48.1	157	517.2	157	517.2	Basalt	3080	10.6	1	15	15	1	91.26
	200	500	450	50	4400	4000	1300	48.1	157	517.2	157	517.2	Basalt	3080	10.6	1	15	15	1	89.1
	200	500	450	50	4400	4000	1300	48.1	157	517.2	157	517.2	Carbon	4320	9.4	1	10	10	1	91.16
	200	500	450	50	4400	4000	1300	48.1	157	517.2	157	517.2	Carbon	4320	9.4	1	10	10	1	93.82
	200	500	450	50	4400	4000	1300	48.1	157	517.2	157	517.2	Glass	2610	8.4	1	25	20	1	88.9
	200	500	450	50	4400	4000	1300	48.1	157	517.2	157	517.2	Glass	2610	8.4	1	25	20	1	89.68

(continued)

Refs	b (mm)	h (mm)	d (mm)	d' (mm)	L (mm)	l (mm)	a (mm)	f_{ck} (MPa)	A_s (mm ²)	f_y (MPa)	A_s' (mm ²)	f_y' (MPa)	Material	f_f (MPa)	A_f (mm ²)	layer	S_{wr} (mm)	S_{wf} (mm)	Anchorage	P_y (kN)
	120	135	118.89	0	1500	1300	450	42.19	142.6	580	0	0	Glass	1789	8.86	3	8	8	0	33.66
	120	135	118.89	0	1500	1300	450	42.19	142.6	580	0	0	Glass	1789	8.86	3	8	8	0	38.22
	120	135	118.89	0	1500	1300	450	42.19	142.6	580	0	0	Glass	1789	17.71	6	8	8	0	34.89
	120	135	118.89	0	1500	1300	450	42.19	142.6	580	0	0	Glass	1789	26.57	9	8	8	0	38.71
[48]	120	135	118.89	0	1500	1300	450	42.19	142.6	580	0	0	RC							29.59
	120	135	118.89	0	1500	1300	450	42.19	142.6	580	0	0	Glass	1789	8.86	3	8	8	0	35.51
	120	135	118.89	0	1500	1300	450	42.19	142.6	580	0	0	Glass	1789	8.86	3	8	8	0	38.46
	120	135	118.89	0	1500	1300	450	42.19	142.6	580	0	0	Glass	1789	26.57	9	8	8	0	35.26
	120	135	118.89	0	1500	1300	450	42.19	142.6	580	0	0	Carbon	4900	2.77	1	10	10	0	36.49
	120	135	118.89	0	1500	1300	450	42.19	142.6	580	0	0	Carbon	4900	2.77	1	10	10	0	34.4
	120	135	118.89	0	1500	1300	450	42.19	142.6	580	0	0	Carbon	4900	8.32	3	10	10	0	40.44
	120	135	118.89	0	1500	1300	450	42.19	142.6	580	0	0	Carbon	4900	8.32	3	10	10	0	42.66
	120	135	118.89	0	1500	1300	450	42.19	142.6	580	0	0	Carbon	4900	16.63	6	10	10	0	41.92

References

- W. Brameshuber, XIX TC 201-TRC (Textile Reinforced Concrete), 1st ed., Aachen, 2006.
- V. Pino, A. Nanni, D. Arboleda, C. Roberts-Wollmann, T. Cousins, Repair of Damaged Prestressed Concrete Girders with FRP and FRCM Composites, *J. Compos. Constr.* 21 (2017) 04016111(1–14). doi: 10.1061/(ASCE)CC.1943-5614.0000773.
- L.N. Koutas, Z. Tetta, D.A. Bournas, T.C. Triantafyllou, Strengthening of Concrete Structures with Textile Reinforced Mortars: State-of-the-Art Review, *J. Compos. Constr.* 23 (2019) 03118001(1–20). doi: 10.1061/(asce)cc.1943-5614.0000882.
- AC434, *Masonry and Concrete Strengthening Using Fabric-reinforced Cementitious Matrix (FRCM) and Steel Reinforced Grout (SRG) Composite Systems*, ICC Evaluation Service Inc, Los Angeles, CA, 2018.
- ACI Committee 549, ACI 549.4R-13: Guide to Design and Construction of Externally Bonded Fabric-Reinforced Cementitious Matrix (FRCM) Systems for Repair and Strengthening Concrete and Masonry Structures, Farmington Hills, Michigan, 2013.
- A. D'Ambrisi, F. Focacci, Flexural strengthening of RC beams with cement-based composites, *J. Compos. Constr.* 15 (2011) 707–720. https://doi.org/10.1061/(ASCE)CC.1943-5614.0000218.
- I.G. Colombo, A. Magri, G. Zani, M. Colombo, M. di Prisco, Textile Reinforced Concrete: experimental investigation on design parameters, *Mater. Struct.* 46 (2013) 1933–1951. https://doi.org/10.1617/s11527-013-0017-5.
- J. Park, S. Hong, S.K. Park, Experimental study on flexural behavior of TRM-strengthened RC beam: various types of textile-reinforced mortar with non-impregnated textile, *Appl. Sci.* 9 (2019) 1–13. https://doi.org/10.3390/app9101981.
- S.P. Yin, S.L. Xu, An Experimental Study on Improved Mechanical Behavior of Textile-Reinforced Concrete, in: *Int. Conf. Struct. Build. Mater.*, 2011: pp. 1850–1853. doi: 10.4028/www.scientific.net/AMR.168-170.1850.
- L.H. Sneed, S. Verre, C. Carloni, L. Ombres, Flexural behavior of RC beams strengthened with steel-FRCM composite, *Eng. Struct.* 127 (2016) 686–699. https://doi.org/10.1016/j.engstruct.2016.09.006.
- C. Escrig, L. Gil, E. Bernat-Maso, Experimental comparison of reinforced concrete beams strengthened against bending with different types of cementitious-matrix composite materials, *Constr. Build. Mater.* 137 (2017) 317–329. https://doi.org/10.1016/j.conbuildmat.2017.01.106.
- S.M. Raoof, L.N. Koutas, D.A. Bournas, Textile-reinforced mortar (TRM) versus fibre-reinforced polymers (FRP) in flexural strengthening of RC beams, *Constr. Build. Mater.* 151 (2017) 279–291. https://doi.org/10.1016/j.conbuildmat.2017.05.023.
- T.G. Wakjira, M. Afzal, U. Ebead, Efficacy of FRCM systems in flexural strengthening of RC T-beams, *IOP Conf. Ser. Mater. Sci. Eng.* 431 (2018) 10.1088/1757-899X/431/7/072007.
- J. Dai, B. Wang, S. Xu, Textile reinforced engineered cementitious composites (TR-ECC) overlays for the strengthening of RC beams, in: *Second Off. Int. Conf. Int. Inst. FRP Constr. Asia-Pacific Reg.*, Seoul, 2009: pp. 75–80. http://www.iifc-hq.org/proceedings/APFIS_2009/PAPER/W1A6.pdf.
- L. Ombres, Debonding analysis of reinforced concrete beams strengthened with fibre reinforced cementitious mortar, *Eng. Fract. Mech.* 81 (2012) 94–109. https://doi.org/10.1016/j.engfracmech.2011.06.012.
- Z.C. Tetta, L.N. Koutas, D.A. Bournas, Textile-reinforced mortar (TRM) versus fiber-reinforced polymers (FRP) in shear strengthening of concrete beams, *Compos. Part B: Eng.* 77 (2015) 338–348. https://doi.org/10.1016/j.compositesb.2015.03.055.
- R. Ortlepp, U. Hampel, M. Curbach, A new approach for evaluating bond capacity of TRC strengthening, *Cem. Concr. Compos.* 28 (2006) 589–597. https://doi.org/10.1016/j.cemconcomp.2006.05.003.
- H.W. Reinhardt, M. Krüger, C.U. Große, Concrete prestressed with textile fabric, *J. Adv. Concr. Technol.* 1 (2003) 231–239. https://doi.org/10.3151/jact.1.231.
- H.D. Nguyen, Q. Zhang, E. Choi, W. Duan, An improved deflection model for FRP RC beams using an artificial intelligence-based approach, *Eng. Struct.* 219 (2020), 110793. https://doi.org/10.1016/j.engstruct.2020.110793.
- B. Taha, P. Muhammad Ali, H. Ahmed, Optimizing the flexural strength of beams reinforced with fiber reinforced polymer bars using back-propagation neural networks, *Aro. Sci. J. Koya Univ.* 3 (2) (2015) 1–10.
- H. Naderpour, D. Rezaadegh Eidgaheh, P. Fakharian, A.H. Rafiean, S.M. Kalantari, A new proposed approach for moment capacity estimation of ferrocement members using Group Method of Data Handling, *Eng. Sci. Technol. an Int. J.* 23 (2020) 382–391. https://doi.org/10.1016/j.jestch.2019.05.013.
- S. Freitag, M. Beer, W. Graf, M. Kaliske, Lifetime prediction using accelerated test data and neural networks, *Comput. Struct.* 87 (2009) 1187–1194. https://doi.org/10.1016/j.compstruc.2008.12.007.
- W. Graf, S. Freitag, M. Kaliske, J.U. Sickert, Recurrent neural networks for uncertain time-dependent structural behavior, *Comput. Civ. Infrastruct. Eng.* 25 (2010) 322–323. https://doi.org/10.1111/j.1467-8667.2009.00645.x.
- S. Freitag, W. Graf, M. Kaliske, J.U. Sickert, Prediction of time-dependent structural behaviour with recurrent neural networks for fuzzy data, *Comput. Struct.* 89 (2011) 1971–1981. https://doi.org/10.1016/j.compstruc.2011.05.013.
- M. Halvaei, M. Jamshidi, M. Latifi, M. Ejtemaei, Effects of volume fraction and length of carbon short fibers on flexural properties of carbon textile reinforced engineered cementitious composites (ECCs); an experimental and computational study, *Constr. Build. Mater.* 245 (2020), 118394. https://doi.org/10.1016/j.conbuildmat.2020.118394.
- M. Halvaei, M. Jamshidi, M. Latifi, M. Ejtemaei, Experimental investigation and modelling of flexural properties of carbon textile reinforced concrete, *Constr. Build. Mater.* 262 (2020), 120877. https://doi.org/10.1016/j.conbuildmat.2020.120877.
- X. Zou, L.H. Sneed, T. D'Antino, Full-range behavior of fiber reinforced cementitious matrix (FRCM)-concrete joints using a trilinear bond-slip relationship, *Compos. Struct.* 239 (2020), 112024. https://doi.org/10.1016/j.compstruct.2020.112024.
- T.G. Wakjira, M. Ibrahim, U. Ebead, M.S. Alam, Explainable machine learning model and reliability analysis for flexural capacity prediction of RC beams strengthened in flexure with FRCM, *Eng. Struct.* 255 (2022), 113903. https://doi.org/10.1016/j.engstruct.2022.113903.
- K. Hornik, M. Stinchcombe, H. White, Multilayer feedforward networks universal approximators, *Neural Networks* 2 (1989) 359–366. https://doi.org/10.1016/0893-6080(89)90020-8.
- E. Tjoa, C. Guan, A Survey on Explainable Artificial Intelligence (XAI): toward medical XAI, *IEEE Trans. Neural Networks Learn. Syst.* 32 (2021) 4793–4813. https://doi.org/10.1109/TNNLS.2020.3027314.
- M.M. Ahsan, M.A.P. Mahmud, P.K. Saha, K.D. Gupta, Z. Siddique, Effect of data scaling methods on machine learning algorithms and model performance, *Technologies* 9 (2021) 52. https://doi.org/10.3390/technologies9030052.
- J. Neyman, On the two different aspects of the representative method: the method of stratified sampling and the method of purposive selection, *J. R. Stat. Soc.* 97 (1934) 558–625. https://doi.org/10.2307/2342192.
- X. Glorot, Y. Bengio, Understanding the difficulty of training deep feedforward neural networks, in: *Proc. Thirteenth. Int. Conf. Artif. Intell. Stat. PMLR*, Chia Laguna Resort, Sardinia, Italy, 2010: pp. 249–256. http://proceedings.mlr.press/v9/glorot10a/glorot10a.pdf.
- V. Nair, G.E. Hinton, Rectified Linear Units Improve Restricted Boltzmann Machines, in: *ICML'10 Proc. 27th Int. Conf. Int. Conf. Mach. Learn.*, Omnipress2600 Anderson StMadisonWIUnited States, Haifa, Israel, 2010: pp. 807–814. doi: https://dl.acm.org/doi/10.5555/3104322.3104425.
- K. He, X. Zhang, S. Ren, J. Sun, Delving deep into rectifiers: Surpassing human-level performance on imagenet classification, in: *2015 IEEE Int. Conf. Comput. Vis.*, Santiago, Chile, 2015: pp. 1026–1034. doi: 10.1109/ICCV.2015.123.
- D.A. Clevert, T. Unterthiner, S. Hochreiter, Fast and accurate deep network learning by exponential linear units (ELUs), in: *4th Int. Conf. Learn. Represent. ICLR 2016*, San Juan, Puerto Rico, 2016: pp. 1–14. doi: doi: 10.48550/arXiv.1511.07289.

- [37] D.P. Kingma, J.L. Ba, Adam: A method for stochastic optimization, in: 3rd Int. Conf. Learn. Represent. ICLR 2015, San Diego, California, USA, 2015: pp. 1–15.
- [38] S.M. Lundberg, S.-I. Lee, A Unified Approach to Interpreting Model Predictions, in: NIPS'17 Proc. 31st Int. Conf. Neural Inf. Process. Syst., Curran Associates Inc. 57 Morehouse Lane Red Hook NY United States, Long Beach California USA, 2017: pp. 4768–4777. doi: <https://dl.acm.org/doi/10.5555/3295222.3295230>.
- [39] E. Štrumbelj, I. Kononenko, An efficient explanation of individual classifications using game theory, *J. Mach. Learn. Res.* 11 (2010) 1–18. doi: [10.5555/1756006.1756007](https://doi.org/10.5555/1756006.1756007).
- [40] M.T. Ribeiro, S. Singh, C. Guestrin, “Why Should I Trust You?” Explaining the Predictions of Any Classifier, in: KDD '16 Proc. 22nd ACM SIGKDD Int. Conf. Knowl. Discov. Data Min., Association for Computing Machinery New York NY United States, San Francisco California USA, 2016: pp. 97–101. doi: [10.1145/2939672.2939778](https://doi.org/10.1145/2939672.2939778).
- [41] A. Shrikumar, P. Greenside, A. Kundaje, Learning important features through propagating activation differences, in: ICML'17 Proc. 34th Int. Conf. Mach. Learn., Sydney NSW, Australia, 2017: pp. 3145–3153. doi: [10.5555/3305890.3306006](https://doi.org/10.5555/3305890.3306006).
- [42] U. Narayanan, A. Unnikrishnan, V. Paul, S. Joseph, A survey on various supervised classification algorithms, in: 2017 Int. Conf. Energy, Commun. Data Anal. Soft Comput., IEEE, Chennai, India, 2017: pp. 2118–2124. doi: [10.1109/ICECDS.2017.8389824](https://doi.org/10.1109/ICECDS.2017.8389824).
- [43] A. Jabr, *Flexural Strengthening of RC beams using Fiber Reinforced Cementitious Matrix, FRCM*, University of Windsor, 2017.
- [44] K. Jung, K. Hong, S. Han, J. Park, J. Kim, Prediction of flexural capacity of RC beams strengthened in flexure with FRP fabric and cementitious matrix, *Int. J. Polym. Sci.* 2015 (2015) 1–11, <https://doi.org/10.1155/2015/868541>.
- [45] T.N.S. Billows, *Flexural Strengthening of Reinforced Concrete Beams with Fabric Reinforced Cementitious Mortar: Effect of Reinforcement Ratios*, University of British Columbia, 2016.
- [46] H.M. Elsanadedy, T.H. Almusallam, S.H. Alsayed, Y.A. Al-Salloum, Flexural strengthening of RC beams using textile reinforced mortar - Experimental and numerical study, *Compos. Struct.* 97 (2013) 40–55, <https://doi.org/10.1016/j.compstruct.2012.09.053>.
- [47] L. Ombres, Flexural analysis of reinforced concrete beams strengthened with a cement based high strength composite material, *Compos. Struct.* 94 (2011) 143–155, <https://doi.org/10.1016/j.compstruct.2011.07.008>.
- [48] J. Park, S. Park, S. Hong, Experimental study of flexural behavior of reinforced concrete beam strengthened with prestressed textile-reinforced mortar, *Materials (Basel)*. 13 (2020) 1–14, <https://doi.org/10.3390/ma13051137>.